6-20-2023

Exploring the Inhibition of the Soluble Lytic Transglycosylase Cj0843c of *Campylobacter jejuni* via Targeting Different Sites with Different Scaffolds

Vijay Kumar
Case Western Reserve University, vxk107@case.edu

Jacob Boorman
Case Western Reserve University, jxb923@case.edu

Focco van den Akker
Case Western Reserve University, fxv5@case.edu

Recommended Citation

Kumar V, Boorman J,Greenlee WJ, Zeng X, Lin J, van den Akker F.Exploring the inhibition of the soluble lytictransglycosylase Cj0843c of Campylobacter jejunivia targeting different sites with different scaffolds.Protein Science. 2023;32(7):e4683. https://doi.org/10.1002/pro.4683

Received: 15 March 2023 | Revised: 4 May 2023 | Accepted: 14 May 2023

DOI: 10.1002/pro.4683

ARTICLE

THE PROTEIN SOCIETY WILEY

Exploring the inhibition of the soluble lytic transglycosylase Cj0843c of *Campylobacter jejuni* via targeting different sites with different scaffolds

Vijay Kumar[1] | **Jacob Boorman**[1] | **William J. Greenlee**[2] | **Ximin Zeng**[3] | **Jun Lin**[3] | **Focco van den Akker**[1]

[1]Department of Biochemistry, Case Western Reserve University, Cleveland, Ohio, USA

[2]MedChem Discovery Consulting, LLC, Teaneck, New Jersey, USA

[3]Department of Animal Science, University of Tennessee, Knoxville, Tennessee, USA

Correspondence
Focco van den Akker, Department of Biochemistry, Case Western Reserve University, Cleveland, OH 44106, USA.
Email: focco.vandenakker@case.edu

Funding information
National Institute of Health, Grant/Award Number: 1R21AI148875

Review Editor: John Kuriyan

Abstract

Bacterial lytic transglycosylases (LTs) contribute to peptidoglycan cell wall metabolism and are potential drug targets to potentiate β-lactam antibiotics to overcome antibiotic resistance. Since LT inhibitor development is underexplored, we probed 15 N-acetyl-containing heterocycles in a structure-guided fashion for their ability to inhibit and bind to the *Campylobacter jejuni* LT Cj0843c. Ten GlcNAc analogs were synthesized with substitutions at the C1 position, with two having an additional modification at the C4 or C6 position. Most of the compounds showed weak inhibition of Cj0843c activity. Compounds with alterations at the C4 position, replacing the -OH with a $-NH_2$, and C6 position, the addition of a $-CH_3$, yielded improved inhibitory efficacy. All 10 GlcNAc analogs were crystallographically analyzed via soaking experiments using Cj0843c crystals and found to bind to the +1 +2 saccharide subsites with one of them additionally binding to the −2 −1 subsite region. We also probed other N-acetyl-containing heterocycles and found that sialidase inhibitors N-acetyl-2,3-dehydro-2-deoxyneuraminic acid and siastatin B inhibited Cj0843c weakly and crystallographically bound to the −2 −1 subsites. Analogs of the former also showed inhibition and crystallographic binding and included zanamivir amine. This latter set of heterocycles positioned their N-acetyl group in the −2 subsite with additional moieties interacting in the −1 subsite. Overall, these results could provide novel opportunities for LT inhibition via exploring different subsites and novel scaffolds. The results also increased our mechanistic understanding of Cj0843c regarding peptidoglycan GlcNAc subsite binding preferences and ligand-dependent modulation of the protonation state of the catalytic E390.

KEYWORDS

bulgecin A, GlcNAc saccharide binding, peptidoglycan metabolism, protein crystallography, soluble lytic transglycosylase, structure-based inhibitor design, β-lactam antibiotic potentiation

1 | INTRODUCTION

Lytic transglycosylases (LTs) are bacterial enzymes that can cleave peptidoglycan (PG) strands of the bacterial cell wall (Dik et al., 2017, 2018; Scheurwater et al., 2008). LTs are needed for cell wall remodeling during cell division, to remove non-crosslinked PG strands to avoid macromolecular crowding and when cells are exposed to β-lactams antibiotics that block PG cross-linking (Weaver et al., 2022). In addition, LTs are needed to make space in the PG layer for nanomachines, such as secretion systems or flagella (Dik et al., 2017). *Escherichia coli* has seven LTs with diverse specificity, including whether they hydrolyze cross-linked versus non-cross-linked PG and whether they have endolytic and/or exolytic activity (Dik et al., 2017; Lee et al., 2013). LTs can be membrane-anchored or soluble, while others bind to secretion systems or flagella (Dik et al., 2017).

LTs are potential drug targets (Chang et al., 2021; Martinez-Bond et al., 2022; Williams et al., 2017) as inhibition of LTs or knocking out LTs has been shown to restore the efficacy of β-lactam antibiotics. This beneficial effect has been shown for a number of serious pathogens, including *E. coli* (Imada et al., 1982), *Neisseria meningitidis* (Williams et al., 2017), *Pseudomonas aeruginosa* (Dik et al., 2019; Horsman et al., 2017; Lee et al., 2018; Tomoshige et al., 2018), *Enterobacter aerogenes* (Tomoshige et al., 2018), *Acinetobacter baumannii* (Tomoshige et al., 2018), *Helicobacter pylori* (Bonis et al., 2012), and *Campylobacter jejuni* (Vijayaraghavan et al., 2018; Zeng et al., 2015). These observed benefits of LT inhibition involve two possible mechanisms that, depending on the pathogen, either or both contribute to the potentiation of β-lactams. In the first mechanism, the penicillin-binding proteins retain glycosyltransferase activity while their PG cross-linking activity is inhibited by β-lactams; this generates long non-cross-linked PG strands (Cho et al., 2014; Weaver et al., 2022). LTs normally clear such non-productive long PG strands; LT inhibition leaves these long PG strands intact, causing the formation of cell wall bulges leading to weak points in the cell wall, making the cell more prone to lysis (Dik et al., 2019; Imada et al., 1982). In the second mechanism, LT activity generates PG disaccharide products (Dik et al., 2017). These products are recycled to the cytoplasm and modified before activating AmpR, which in turn increases β-lactamase expression in pathogens such as *P. aeruginosa*, *Neisseria gonorrhoeae*, and *E. cloacae* (Dik et al., 2017; Dominguez-Gil et al., 2016; Zeng & Lin, 2013). Thus, the inhibition of LT re-sensitizes bacteria to β-lactams by lowering β-lactamase expression.

There are additional benefits of LT inhibition as LTs increase fitness in *A. baumannii* (Crepin et al., 2018) and are needed for toxin release in *Clostridium difficile* (El Meouche & Peltier, 2018; Wydau-Dematteis et al., 2018). Inhibition or deletion of LTs also can lead to increased susceptibility to the host immune system (Perez Medina & Dillard, 2018; Ragland et al., 2017). Furthermore, an antibody against an LT from *S. aureus* enhanced the host immune defense (Lorenz et al., 2011). Also, LTs are critical for sporulation in *Bacillus anthracis* and *C. difficile* (Nocadello et al., 2016) and downregulate immune response signaling in response to *N. gonorrhoeae* (Knilans et al., 2017). LTs are also vital for creating space in the PG for inserting type III secretion systems and flagella; interfering with either process decreases bacterial virulence (Burkinshaw et al., 2015; Roure et al., 2012). Finally, the inactivation of LTs in *Stenotrophomonas maltophilia* leads to increased susceptibility to non-β-lactam antibiotics aminoglycosides and macrolides, likely due to increased membrane permeability due to LT inhibition (Wu et al., 2016).

Tool compounds to probe LT-related mechanistic questions that might be starting points for drug development are very limited, with only bulgecin A showing promising potency. Bulgecin A is a natural product isolated from *P. acidophila* and *P. mesoacidophila* (Imada et al., 1982), and is a relatively broad-spectrum LT inhibitor (Dik et al., 2019; Fibriansah et al., 2012; Imada et al., 1982; Kraft et al., 1999; Nakao et al., 1986; Romeis et al., 1993; Skalweit & Li, 2016; Templin et al., 1992; Thunnissen et al., 1995; Tomoshige et al., 2018; van Asselt et al., 2000; Vijayaraghavan et al., 2018; Williams et al., 2017; Zahrl et al., 2005). A second LT inhibitor is NAG-thiazoline (Reid, Blackburn, & Clarke, 2004; Reid, Blackburn, Legaree, et al., 2004), but it inhibits only one LT, MltB; for example, it does not inhibit *E. coli* MltE (Byun et al., 2018). Thionine acetate was shown to inhibit Slt35 (Mezoughi et al., 2021). Unlike the last two inhibitors, only bulgecin A has been crystallographically confirmed to inhibit LTs (Fibriansah et al., 2012; Lee et al., 2018; Thunnissen et al., 1995; Vijayaraghavan et al., 2018; Williams et al., 2017).

While bulgecin A shows promising effects against different LTs from different organisms in either biochemical

or microbiological assays, virtually no follow-up studies advancing this compound or more potent derivatives have been reported. This is likely due to bulgecin A being very difficult to chemically synthesize as it is carbohydrate-based and has eight chiral centers (Tomoshige et al., 2018). Furthermore, in the only animal study, bulgecin A synergized with a β-lactam antibiotic yielding only a small but significant decrease in colonization of *H. pylori* in mice (Bonis et al., 2012). The small effect was attributed to the instability of bulgecin A in mice (Bonis et al., 2012), further illustrating the need to develop different inhibitors. Also, in *P. aeruginosa*, bulgecin A was found to have poor penetration (Kim et al., 2023). Therefore, new inhibitor tool compounds with different scaffolds are needed to facilitate chemical synthesis and modification by medicinal chemistry to pursue specific or broad-spectrum LT inhibition in vitro and in vivo. Our inhibitor design studies presented herein targeted the LT Cj0843c from *C. jejuni* for the following reasons: (1) its crystals can diffract to 1.87 Å resolution; (2) crystallizes in two space groups; (3) is amenable to ligand soaking experiments; (4) is similar to other donut-shaped soluble LTs like Slt70; (5) its interactions with PG have been studied by molecular dynamics (MD) simulations, mutagenesis, and PG mimicking saccharide soaks; and (6) binding and/or inhibition by bulgecin A can be detected crystallographically, biophysically using thermal shift assay, and enzymatically (Kumar, Mathure, et al., 2021; Vijayaraghavan et al., 2018).

To design new LT inhibitors, we focused on maintaining a moiety that bulgecin A (Figure 1) and the PG substrate share and that is an N-acetyl-group containing a six-membered ring, that is, N-acetyl-glucosamine (GlcNAc). The GlcNAc moiety and N-acetylmuramic acid, which is GlcNAc with a lactic acid moiety, are alternating PG strand building blocks; the N-acetylmuramic acid building blocks in PG are linked to peptide moieties. Crystallographic studies of di- and trisaccharides of GlcNAc bound to Cj0843c showed di- and trisaccharides binding in two locations in the active site groove (Kumar, Mathure, et al., 2021). These saccharide binding sites are on either side of the catalytic E390 where PG cleavages take place; GlcNAc moieties in the −2 and +1 subsites make the most interactions compared to the moieties in the other subsites (Kumar, Mathure, et al., 2021). To develop new LT inhibitors, we generated GlcNAc derivatives to explore interactions in the Cj0843c active site. In addition, we modified the GlcNAc scaffold at two different positions using structure-guided ligand design. Finally, we probed N-acetyl-containing molecules that have a different six-membered heterocyclic ring. Overall, 15 compounds were probed for their inhibition of Cj0843c LT, and their binding modes were crystallographically investigated (Figure 1).

2 | RESULTS

2.1 | Cj0843c compound inhibition studies

Based on initial docking calculations that probed the binding of five potential analogs of GlcNAc to Cj0843c (Supporting Information: Figure S1), these five and an additional set of three GlcNAc analogs each with different substituents at the O1 position (LV8036, LV8044, LV8060, Z7146, Z7912, Z7285, Z3252, and Z3261) were synthesized via Supporting Information: Scheme 1. Also, two analogs of LV8060, Fv17b, and Fv16b, were synthesized. This first analog, Fv17b, replaces the -OH group at the ring C4 position with a -NH_2 group (Supporting Information: Figure S3 for synthesis details). The -OH at this position in GlcNAc positioned in the +1 subsite hydrogen bonds with E390 (Kumar, Mathure, et al., 2021), so the introduced amine was designed to form a potential salt-bridge interaction with E390. Residue E390 is speculated to be protonated/neutral during a key step in catalysis based on mechanistic analyses of this and related LTs but could be deprotonated/charged in other steps (Byun et al., 2018; Kumar, Mathure, et al., 2021; Thunnissen et al., 1995; Vijayaraghavan et al., 2018). A charged E390 could be the reason why bulgecin A is quite a potent LT inhibitor since it positions a positively charged secondary amine at 3.6 Å distance from E390 (Vijayaraghavan et al., 2018). A second analog of LV8060, Fv16b, was synthesized by adding a -CH_3 to the oxygen at the C6 position (Supporting Information: Figure S3 for synthesis) to promote hydrophobic and/or van der Waals interactions with several residues involving the Cγ atom of E498, the side chains of I501 and Y502, and main chain atoms of I502-E498 which are in an α helix. Finally, an additional GlcNAc analog was purchased for testing, 4-nitrophenyl N,N′-diacetyl-β-D-chitobioside. The GlcNAc analogs were tested for their ability to inhibit Cj0843c (Figure 2). The compounds show only modest inhibition, with Fv16b and Fv17b being the most pronounced at the highest concentrations tested (low mM). An IC_{50} could not be calculated from these dose–response measurements for any of the tested compounds due to their weak affinities as the inhibition had not plateaued at the higher concentrations used in the experiments.

In addition to the above-mentioned synthesized compounds, we purchased three compounds that have a different six-membered heterocyclic ring with an N-acetyl group substituent: N-acetyl-2,3-dehydro-2-deoxyneuraminic acid, siastatin B, and zanamivir amine. These compounds were tested for their ability to inhibit Cj0843c (Figure 2). An analog of N-acetyl-

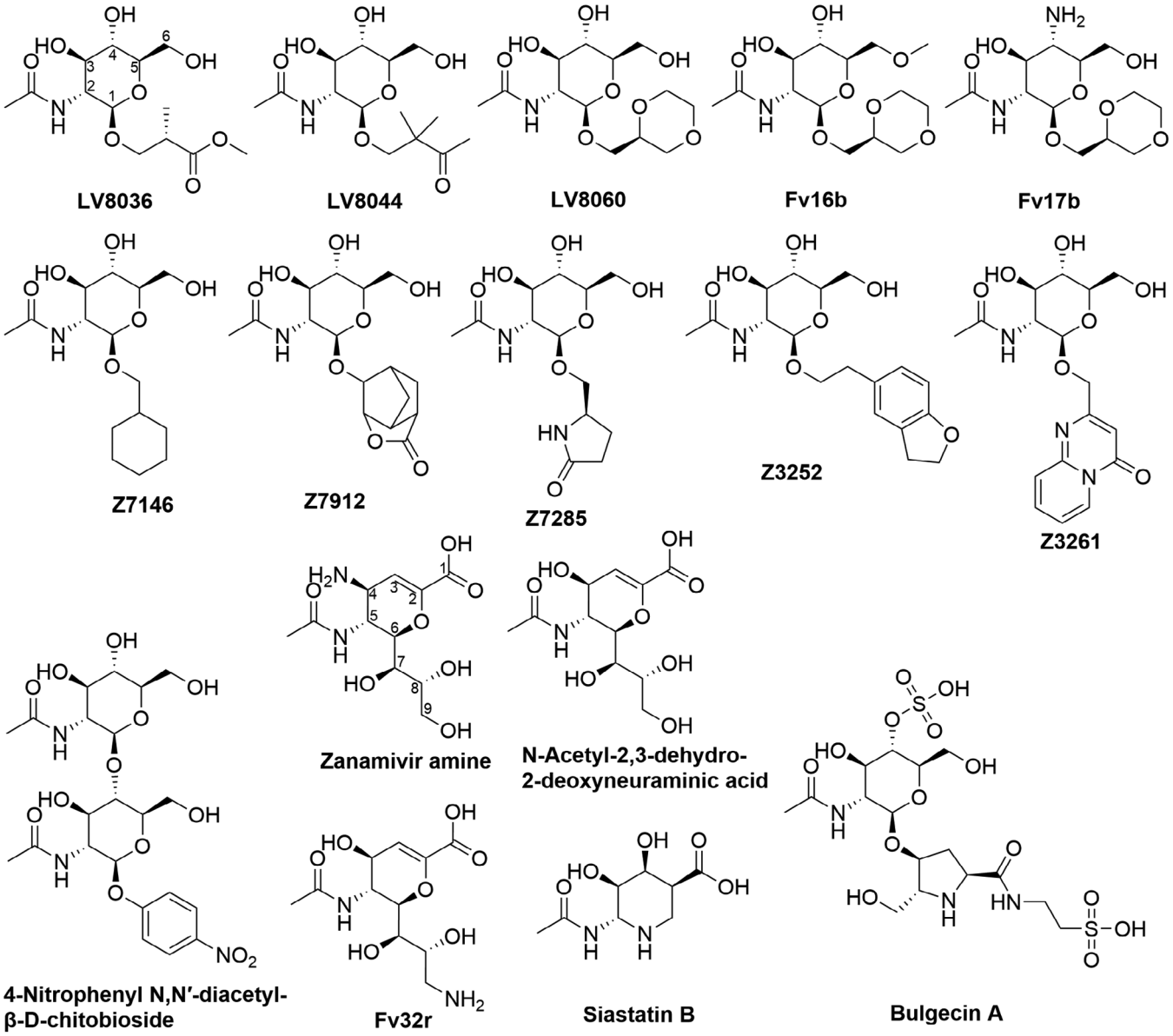

FIGURE 1 Chemical structures of compounds used in the study. The carbon numbering for the GlcNAc moiety of LV8036 is shown; the carbon numbering for zanamivir amine is also shown.

2,3-dehydro-2-deoxyneuraminic acid was designed and synthesized, Fv32r, to replace the primary -OH group with an -NH_2 aimed to make a salt bridge interaction with E390. This analog showed modest inhibition at the higher concentrations tested (Figure 2). For comparison with the 15 analyzed inhibitors, we tested bulgecin A at 75 μM, which yielded 0.57 ± 0.2 fractional activity of uninhibited Cj0843c, thus decreasing the activity by 43%. This close to 50% inhibition of Cj0843c observed for 75 μM bulgecin A is within a factor of 3 of the previously measured K_d of 210 μM for bulgecin A binding to Cj0843c using the thermal shift assay/differential scanning fluorimetry (Vijayaraghavan et al., 2018).

2.2 | Crystallographic analysis of compound binding

We characterized the binding of the compounds by soaking the compounds at 10 mM in crystals of Cj0843c and determined the crystal structures of the complexes. All 15 compounds showed crystallographic evidence of binding to the active site of Cj0843c (Figures 3 and 4).

2.3 | GlcNAc analogs

All GlcNAc analogs bound only in the +1 +2 subsites except for Z7285, for which two molecules were bound in

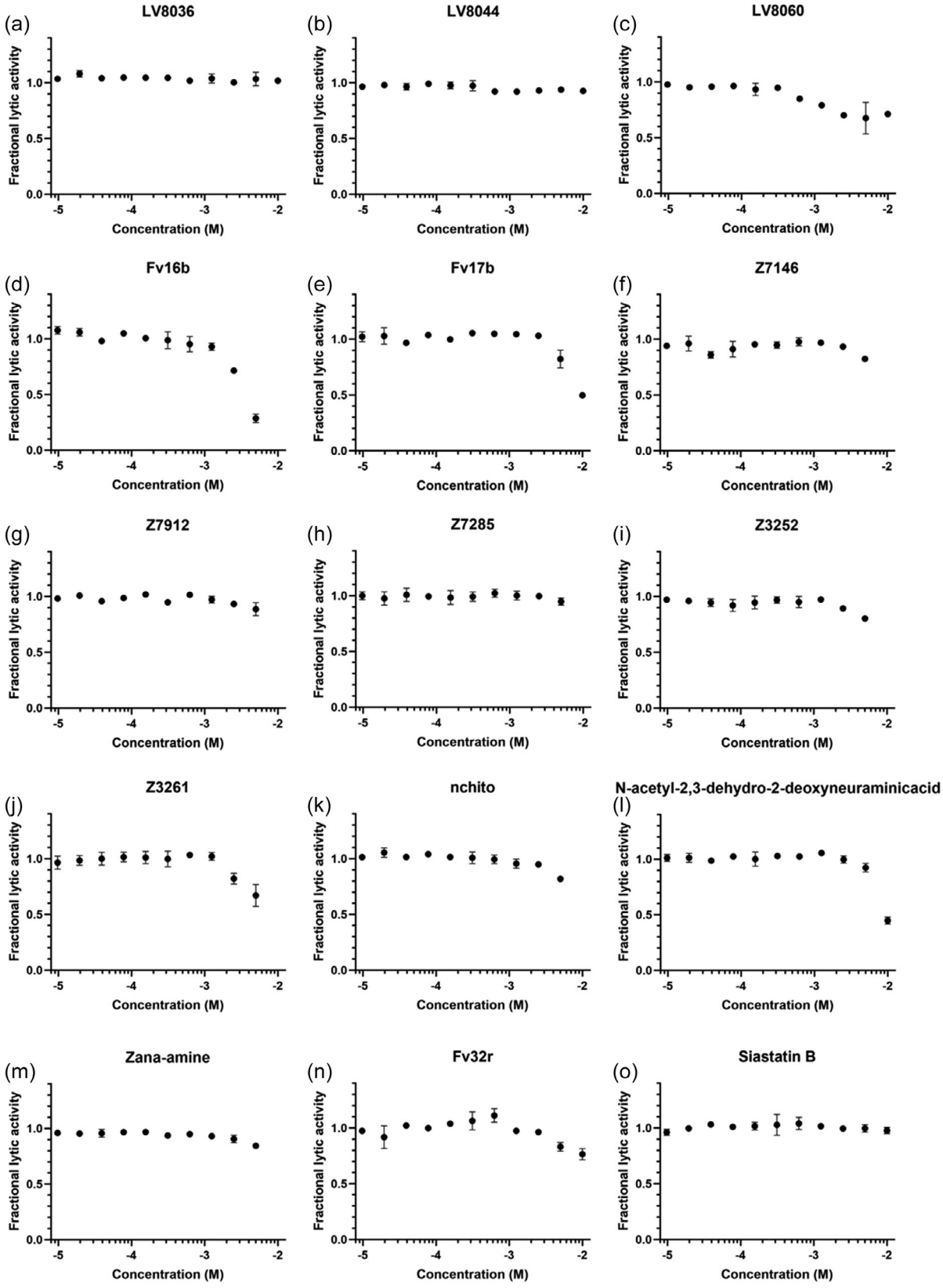

FIGURE 2 Dose–response lytic transglycosylase activity of Cj0843c testing 15 inhibitors. Data are plotted as fractional lytic activity, with 1.0 being uninhibited. Panels (a–o) show Cj0843c inhibition by inhibitors LV8036, LV8044, LV8060, Fv16b, Fv17b, Z7146, Z7912, Z7285, Z3252, Z3261, 4-nitrophenyl N,N′-diacetyl-β-D-chitobioside, N-acetyl-2,3-dehydro-2-deoxyneuraminic acid, zanamivir amine, Fv32r, and siastatin B, respectively.

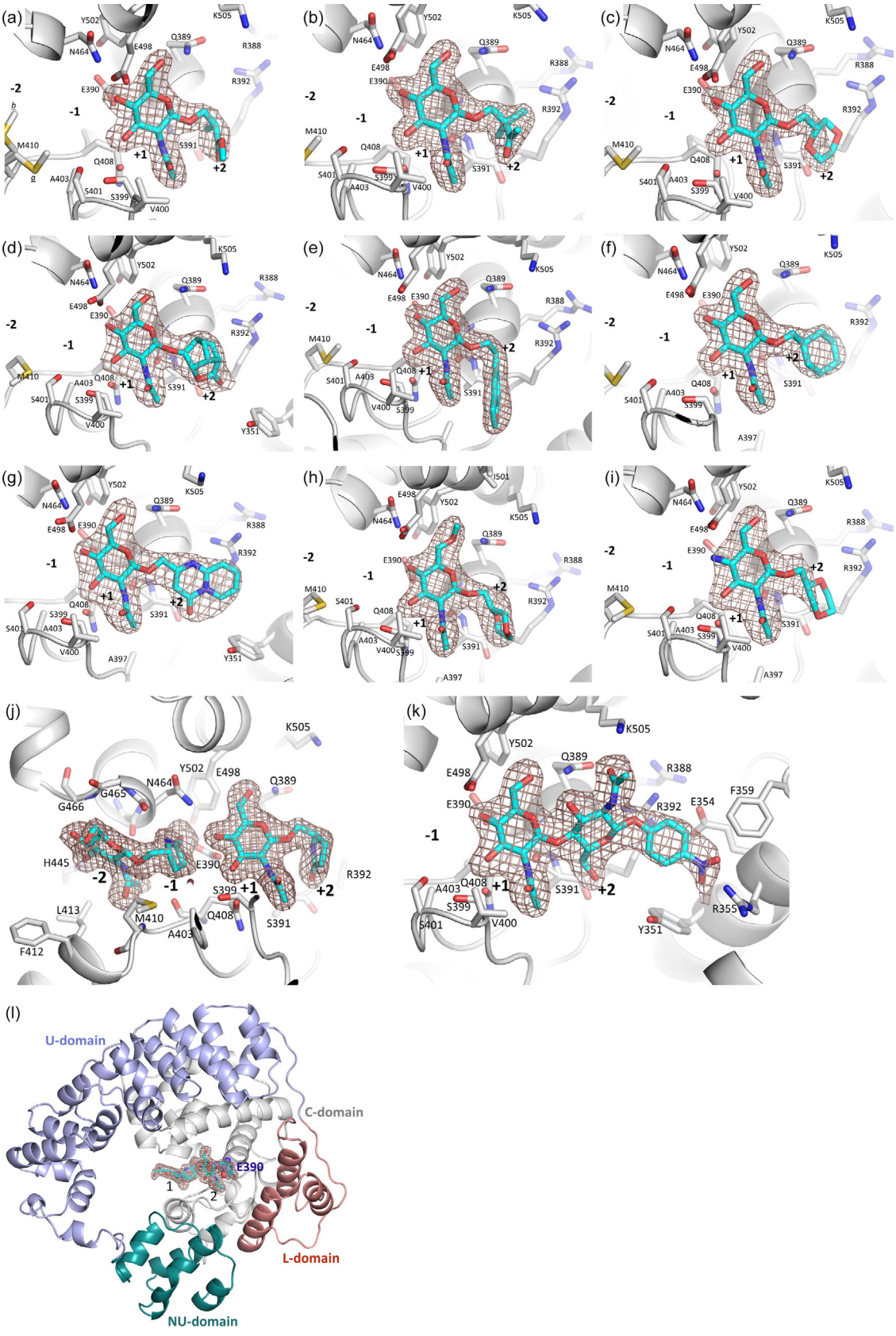

FIGURE 3 Legend on next page.

the active site (the +1 +2 and −2 −1 subsites; Figure 3). The compounds all bind to the PG-binding groove on the inner surface of the doughnut-shaped Cj0843c (as illustrated for the two molecules of Z7285 binding to Cj0843c in Figure 3l). The interactions of the GlcNAc moieties in the +1 subsites all involve hydrogen bonds of the N-acetyl group nitrogen with the backbone oxygen of E390, the O3 hydroxyl with Q408, the O4 hydroxyl with E390, and the O6 hydroxyl with the amide nitrogen of the Q389 side chain (Figure 5). The latter interaction likely involves a hydrogen bond accepting interaction by the O6 hydroxyl as the orientation of the amide moiety of the Q389 side chain is deduced from analysis of the hydrogen-bonding network of the water that interacts with the oxygen of the Q389 side chain and other interacting atoms which are all hydrogen bond donors (R388, R392, and the nitrogen of the N509 side chain). The GlcNAc O1 substituents are situated in the +2 subsite, which harbors the C-terminal end of the α-helix comprising residues 377–390 (Figure 5). This +2 subsite region is relatively hydrophobic due to the main chain conformation of S391 and R392; the +2 subsite harbors the nonpolar face of residues 391–392, the Cβ and Cγ atoms of R392, and Y351. The O1 substituents do not make direct hydrogen bond interactions; Z3253, Fv17b, and Z7285 do however make water-mediated hydrogen bonds (Figure 5e,i,j, respectively).

The designed Fv16b compound binds as intended by maintaining its four GlcNAc hydrogen bonds (Figure 5h). This includes the O6 atom, which is now an ether in Fv16b instead of an alcohol; this O6 hydrogen bond acceptor atom is making a 2.9 Å hydrogen bonding interaction with the nitrogen of the Q389 side chain (Figure 5h). The added methyl at the O6 position makes hydrophobic interactions with the Cγ atom of E498 (3.9 Å), Cα of Y502 (4.3 Å), and is slightly more distant from the Cγ2 atom of I501 (4.5 Å; Figure 5h).

The design of the methyl addition to the O6 atom of GlcNAc to improve affinity for Cj0843c could also be tried in other LTs as the GlcNAc moieties from reaction products or PG fragments bind identically in their respective +1 subsites (Supporting Information: Figure S4; van Asselt et al., 1999). In addition, the hydrophobicity of the residues in the region where the O6 methyl is introduced is relatively conserved: residues E498 and Y502 are highly conserved in four LTs (Supporting Information: Figure S4; van Asselt et al., 1999). Furthermore, I501 in Cj0843c is a G586 in *E. coli* Slt70, and although the other LTs have more polar residues at this position, Q609 in *P. aeruginosa* Slt, R191 in *E. coli* MltE, and D583 in *N. meningitidis* LtgA, in each case these residues position their hydrophobic Cγ and/or Cβ atoms facing this hydrophobic region (Supporting Information: Figure S4b–d; van Asselt et al., 1999).

Like Fv16b, Fv17b also binds as anticipated (Figure 5i). The -NH_2 group introduced at the C4 position in Fv17b is making a 3.0 Å interaction with E390, likely a salt bridge interaction (Figure 5i). The possibility of such a salt bridge with E390, a stronger interaction than a hydrogen bond, agrees with the improved inhibition of Fv17b over LV8060. Like for Fv16b, the Fv17b design could also be tried for inhibitor design in other LTs since the catalytic glutamic acid is conserved.

Superimposing the GlcNAc analog-bound Cj0843c structures reveals that their GlcNAc moieties are situated in the same +1 subsite positions, yet their O1 substituent position varies depending on the nature of the substituents (Figure 6). Although the GlcNAc rings show minimal variation in their position, one of the compounds has its ring slightly more shifted regarding its C4 and C6 groups, which is Fv17b (Figure 6). This perhaps significant shift in the Fv17b saccharide ring could be due to the -NH_2 at the ring C4 position instead of the -OH. Alternatively, the shift could be merely due to the more modest resolution of this 2.48 Å resolution Fv17b Cj0843c complex structure. The superposition includes the substrate-mimicking GlcNAc trisaccharide-bound Cj0843c structure (Kumar, Mathure, et al., 2021), indicating that the analogs' GlcNAc moiety in the +1 subsite makes PG substrate-like interactions.

One of the GlcNAc analogs, Z7285, was bound in two locations in the active site, including the −2 −1 subsites (Figures 3j and 5j). This latter binding mode for Z7285 was similar to that obtained by docking calculations

FIGURE 3 Unbiased omit electron density of GlcNAc-containing inhibitors bound in the Cj0843c active site. Electron density was calculated after the removal of the inhibitors from the model, followed by 10 cycles of Refmac refinement. Density is contoured at the 3 σ level. The inhibitors are shown in stick model with cyan-colored carbon atoms; the protein is shown in a cartoon representation with nearby residues labeled and shown in the stick model. Alternative side-chain conformations are labeled *a* and *b*. The saccharide subsites at labeled in bold (e.g., **+1**). (a) LV8046. (b) LV8044. (c) LV8060. (d) Z7912. (e) Z3252. (f) Z7146. (g) Z3261. (h) Fv16b. (i) Fv17b. (j) Z7285 with two inhibitors bound in the active site. (k) 4-nitrophenyl N,N′-diacetyl-β-D-chitobioside. (l) Zoomed-out view of the doughnut-shaped Cj0843c with two Z7285 molecules bound in the active site. The two Z7285 molecules (labeled 1 and 2 in the −2 −1 and +1 +2 subsites, respectively) are shown as stick with cyan carbon atoms. The N-terminal NU domain (teal), U domain (light blue), L domain (pale red), and catalytic C domain (gray) are shown. The catalytic E390 is depicted as spheres with purple carbon atoms.

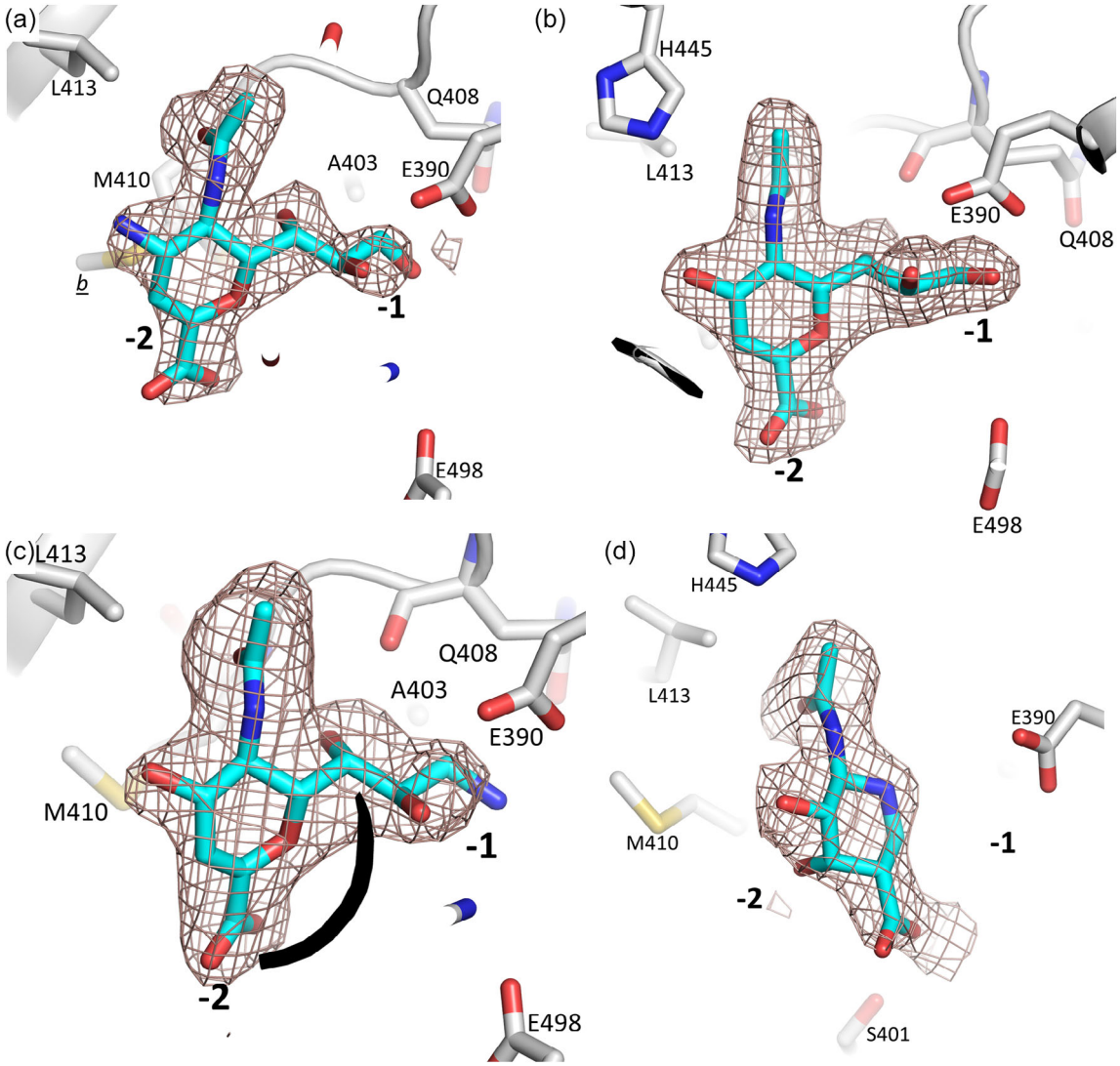

FIGURE 4 Unbiased omit electron density of siastatin B and deoxy-neuraminic acid analogs bound in the Cj0843c active site. Density, inhibitor, and protein representation are in Figure 3. (a) Zanamivir amine. (b) N-acetyl-2,3-dehydro-2-deoxyneuraminic acid. (c) Fv32r. (d) Siastatin B.

(Supporting Information: Figure S1). The nitrogen atom of the 2-pyrrolidinone moiety of Z7285 makes a 3.0 Å hydrogen bond with the backbone oxygen of N464 (Figure 5j). Also, the carbonyl oxygen of the 2-pyrrolidinone moiety of Z7285 makes hydrogen bonds with N464 and E390 (3.2 and 2.3 Å distance, respectively). This latter interaction suggests that E390 is protonated, being the hydrogen bond donor for this interaction with the carbonyl oxygen of Z7285.

To gain insights into the individual affinities of the two Z7285 binding sites, we carried out a dose–response-type soaking experiment where we lowered the concentration from our initial 10 mM to 3 and 1 mM and subsequently collected two additional diffraction data sets. Refinement of the 3 and 1 mM Z7285 soaked Cj0843c structures, and subsequent analysis of the unbiased active site density revealed that at 1 mM, no strong ligand density was present for either binding mode (Supporting Information: Figure S5). For the 3 mM-soaked data set, only strong Z7285 density was observed for the +1 +2 subsites (Supporting Information: Figure S5). These results indicate that the +1 +2 binding site has a higher affinity for Z7285 with an estimated in-crystal affinity between 1 and 3 mM, whereas the −2 −1 subsite is estimated to have an in-crystal affinity between 3 and 10 mM. These Z7285 dose–response soaking experiments agree with an analysis of the temperature factors of the ligand and protein atoms in the 10 mM Z7285 Cj04843c complex using color-ramping (Supporting Information: Figure S6). This analysis indicates that the moiety with the lowest ligand temperature factors is the GlcNAc moiety in the +1 subsite, suggesting it is the more ordered moiety.

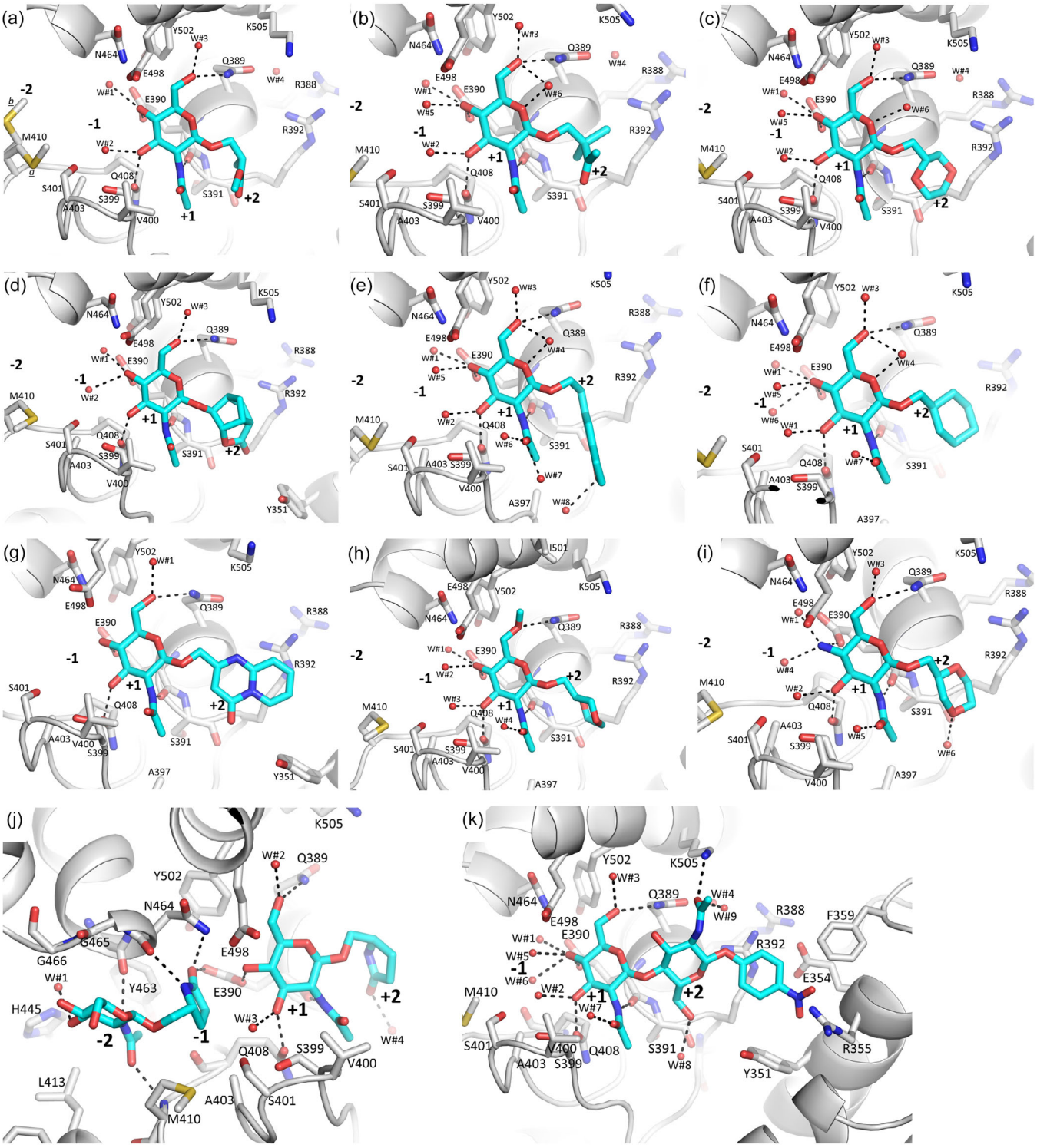

FIGURE 5 Interactions of GlcNAc-containing inhibitors bound in the Cj0843c active site. Inhibitor and protein representation are as in Figure 3, with hydrogen bonds depicted as dashed lines. Water molecules are shown as red spheres and are labeled "W#x." Panels (a–k), same inhibitors as in Figure 3a–k.

The above results indicate that the +1 +2 subsites can more readily bind GlcNAc-containing molecules compared to the −2 −1 subsites. This preference could be due to the larger number of hydrogen bonds GlcNAc makes in the +1 versus the −2 subsite (4 and 2, respectively). This unanticipated preference of GlcNAc analogs for the +1 +2 subsites likely affected the docking predictions that targeted the −2 −1 subsites where bulgecin A

binds. Of the five molecules that were initially predicted, via docking, to bind to the −2 −1 subsites to position an oxygen atom to interact with E390 (LV8036, LV8044, LV8060, Z7912, and Z7285; Supporting Information: Figure S1), only Z7285 bound in this subsite region and the +1 +2 subsites whereas the others only bound in the +1 +2 subsite region (Figure 5). The oxygen atoms of the different substituents at the O1 position that are docked and predicted to form hydrogen bonds with the protonated E390 are in close proximity to the GlcNAc moiety binding to the +1 subsite (Supporting Information: Figure S1). In particular, these oxygen atoms predicted to interact with E390 are in close proximity to the +1 subsite GlcNAc hydroxyl at the C4 position (Supporting Information: Figure S1) that also hydrogen bonds to the same E390 (Figure 5). The docked binding modes in the −2 −1 subsite region would be, therefore, sterically hindered by a second GlcNAc analog also binding to the +1 +2 subsites unless the O1 substituent is small enough to shift over as occurred for Z7285 (Figure 5j and Supporting Information: Figure S1a).

In addition to steric hindrance, the binding of a GlcNAc analog to the +1 position could influence the protonation state of E390 as suggested by MD simulations or, if protonated, perhaps affect which oxygen atom of E390 harbors the proton, thus further complicating future docking endeavors. An additional complicating factor regarding the protonation state of E390 is that the pH of 7.5 of the assay is somewhat higher than the pH of 5.9 used for the soaking experiments. This 1.6 pH unit difference together with the chemical differences of the inhibitors of which some of them are aimed to influence the protonation state of E390 further complicate computational inhibitor design for LTs. For instance, MD simulations of Cj0843c with a PG strand substrate bound suggested that E390 is protonated, whereas MD simulations with di- and trisaccharides of GlcNAc bound in the +1 subsite, mimicking the product-bound state, indicated E390 is deprotonated (Kumar, Mathure, et al., 2021; Vijayaraghavan et al., 2018); these changes in catalytic Glu protonation state were also previously postulated for Slt70 (Thunnissen et al., 1995).

2.4 | Zanamivir amine analogs and siastatin B

N-acetyl-2,3-dehydro-2-deoxyneuraminic acid, zanamivir amine, and siastatin B were all crystallographically observed to bind to the −2 subsite active site region of Cj0843c extending into the −1 subsite (Figures 4 and 7). Based on the observed N-acetyl-2,3-dehydro-2-deoxyneuraminic acid and zanamivir amine interactions, Fv32r was designed and synthesized to replace

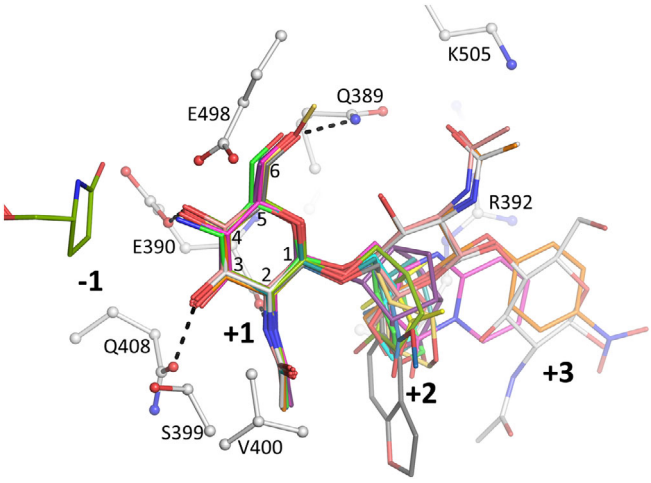

FIGURE 6 Superposition of GlcNAc-containing compounds and analogs bound in the +1 +2 subsites of Cj0843c. The following molecules are shown with the color of their carbon atoms listed in parentheses: GlcNAc trisaccharide (PDBid 7LAM; Kumar, Mathure, et al., 2021); gray; also bound in −2 −3 −4 subsites), GlcNAc disaccharide (PDBid 7LAQ; Kumar, Mathure, et al., 2021); pink; also bound in +1 and +2 subsites), Fv17b (green), LV8060 (cyan), 4-nitrophenyl N,N′-diacetyl-β-D-chitobioside (orange), Z3252 (dark gray), Z3261 (pink), Z7146 (blue green), Z7285 (green, also bound in +2 +1 subsites), Z7912 (purple), Fv16b (golden yellow), LV8036 (dark blue), and LV8044 (yellow). The carbon numbering for GlcNAc in the +1 subsite is shown. Nearby protein residues are shown in ball-and-stick representation (with gray carbon atoms), and conserved hydrogen bonds are depicted as dashed lines.

the terminal -OH with an -NH_2 group to introduce a salt bridge interaction with E390. Fv32r is bound to the same active site region in a similar fashion (Figures 4 and 7). Siastatin B is also bound in the −2 subsite region and has a secondary amine in its 6-membered ring instead of an oxygen as the other compounds. All the compounds position their N-acetyl group in the same pocket with the amide oxygen and nitrogen atoms interacting with the main chain nitrogen of M410 and the oxygen atom of Y463, respectively. These are the same interactions that the N-acetyl group of GlcNAc of bulgecin A and the di- and trisaccharides make in the −2 subsite of the Cj0843c active site (Kumar, Mathure, et al., 2021; Vijayaraghavan et al., 2018). The glycerol substituent at position 6 of zanamivir amine and N-acetyl-2,3-dehydro-2-deoxyneuraminic acid makes hydrogen bonds with the backbone oxygen of Q408 and the E390 side chain (Figure 7). The primary alcohol group at the C9 position also interacts with E390 in the N-acetyl-2,-3-dehydro-2-deoxyneuraminic acid complex but is more disordered in the zanamivir amine complex

(Figures 4c and 7c). The interactions of Fv32r are similar as compared to N-acetyl-2,3-dehydro-2-deoxyneuraminic acid with the introduced -NH_2 group also interacting with E390, likely forming a salt bridge interaction (Figure 7c).

Siastatin B also makes N-acetyl group-mediated hydrogen bonds with the backbone oxygen of M410 (3.0 Å) and backbone nitrogen of Y463 (3.3 Å; Figure 7d). In addition, siastatin B, via its secondary amine ring nitrogen, makes a 2.8 Å hydrogen bond with the backbone oxygen of Q408 (Figure 7d). This secondary amine ring nitrogen is also at 4.5 Å distance from E390 potentially making an electrostatic interaction. Finally, siastatin B makes hydrophobic interactions with A403 and two water-mediated interactions.

Comparison of all the compounds observed to bind to the −2 subsite of Cj0843c reveals a range of different orientations of the N-acetyl-containing six-membered heterocyclic rings (Figure 8). These compounds maintain their N-acetyl amide group active site hydrogen bonds yet reorient the ring as well as the methyl group of the N-acetyl moiety (Figure 8). The apparent pivot point centers around the amide (maintaining hydrogen bonds with M410 and Y463) with the rings of Z7285 and siastatin B being the two extremes of the varying compound orientations. For the Z7285 complex, its six-membered ring is closer to the −3 subsite than any other compounds, whereas the ring in siastatin B is mostly situated in the −1 subsite (Figure 8). The methyl moiety of the N-acetyl group is situated in a hydrophobic pocket comprised of Y463, F409, L413, and H445, and its position varied by as much as 1.5 Å among the different compounds.

3 | DISCUSSION

Fifteen new Cj0843c inhibitors are presented herein, whose binding modes are all crystallographically confirmed. Their apparent affinities are all relatively weak and likely to be in the low mM range, but all are stoichiometrically bound when crystals are soaked at 10 mM concentrations suggesting their K_d values are below 10 mM. The inhibition data using the EnzChek assay suggests a similar mM affinity for the inhibitors. Despite their low affinity, this study is the first advancement of new inhibitors for LTs that have been crystallographically confirmed since bulgecin A. The broad-spectrum LT inhibitor bulgecin A is a natural product and was discovered in 1982 (Imada et al., 1982), found to inhibit LTs in 1992 (Templin et al., 1992), and crystallographic binding to an LT confirmed in 1995 (Thunnissen et al., 1995) and later in other LTs (Fibriansah et al., 2012; Lee et al., 2018; Vijayaraghavan et al., 2018; Williams et al., 2017). The eight chiral centers of this natural product leading to the difficulty of chemically synthesizing bulgecin A has likely hampered the field in finding novel analogs (Tomoshige et al., 2018). Our studies have shown that Cj0843c-inhibiting derivatives of O1-substituted GlcNAc molecules can be relatively easily synthesized. In addition, modification of the GlcNAc scaffold by changes at the carbon 4 and 6 positions (Fv17b and Fv16b, respectively) improve inhibitory potency. Furthermore, in addition to the GlcNAc scaffold, compounds with two different yet related scaffolds were found to inhibit Cj0843c: zamamivir amine (and analogs) and siastatin B. Comparing N-acetyl-2,3-dehydro-2-deoxyneuraminic acid and Fv32r, the change of the -OH to -NH_2 at the C9 position to make a salt-bridge interaction with E390 did not seem to increase affinity possibly due entropic considerations of the rotational freedom around the C8-C9 bond. Comparing N-acetyl-2,3-dehydro-2-deoxyneuraminic acid and zanamivir amine, the change of the -OH to -NH_2 at the C4 position to generate a possible favorable helix dipole interaction (Hol, 1985), being near the C-terminus of the α helix comprising residues 456–464, did not improve inhibition.

Our studies show that compounds binding to the −2 and +1 subsite regions can inhibit an LT, indicating that both regions can be exploited for LT inhibitor design. The Cj0843c inhibitor studies also suggest that the +1 subsite has a higher affinity for GlcNAc moieties than the −2 subsite as only one analog bound in the latter region while also still binding to the +1 subsite region.

The ability of neuraminidase/sialidase inhibitors siastatin B (Kudo et al., 1993; Tailford et al., 2015), N-acetyl-2,3-dehydro-2-deoxyneuraminic acid (Magesh et al., 2008), Fv32r (previously also synthesized as 4-amino-DANA (Smith et al., 2001)), and the zanamivir precursor zanamivir amine (Caceres et al., 2022) to inhibit Cj0843c suggests that such inhibitors could be starting points for design of more-potent LT inhibitors. Zanamivir is FDA-approved to treat flu, and many sialidase inhibitor analogs have previously been synthesized (Keil et al., 2022; Laborda et al., 2016), which could be tested for their ability to inhibit LTs.

The inhibitor results presented herein also increase our mechanistic understanding of Cj0843c. Three pieces of evidence point to that the +1 binding subsite has a higher affinity for binding GlcNac than the −2 subsite; this could be important for what part of a PG strand binds first to the Cj0843c active site. First, only one GlcNAc analog was found to bind in the −2 subsite, whereas all 11 GlcNAc compounds bound to the +1 subsite (Figure 2). Second, the dose–response soaking experiment of Z7285 indicated a higher affinity for the +1

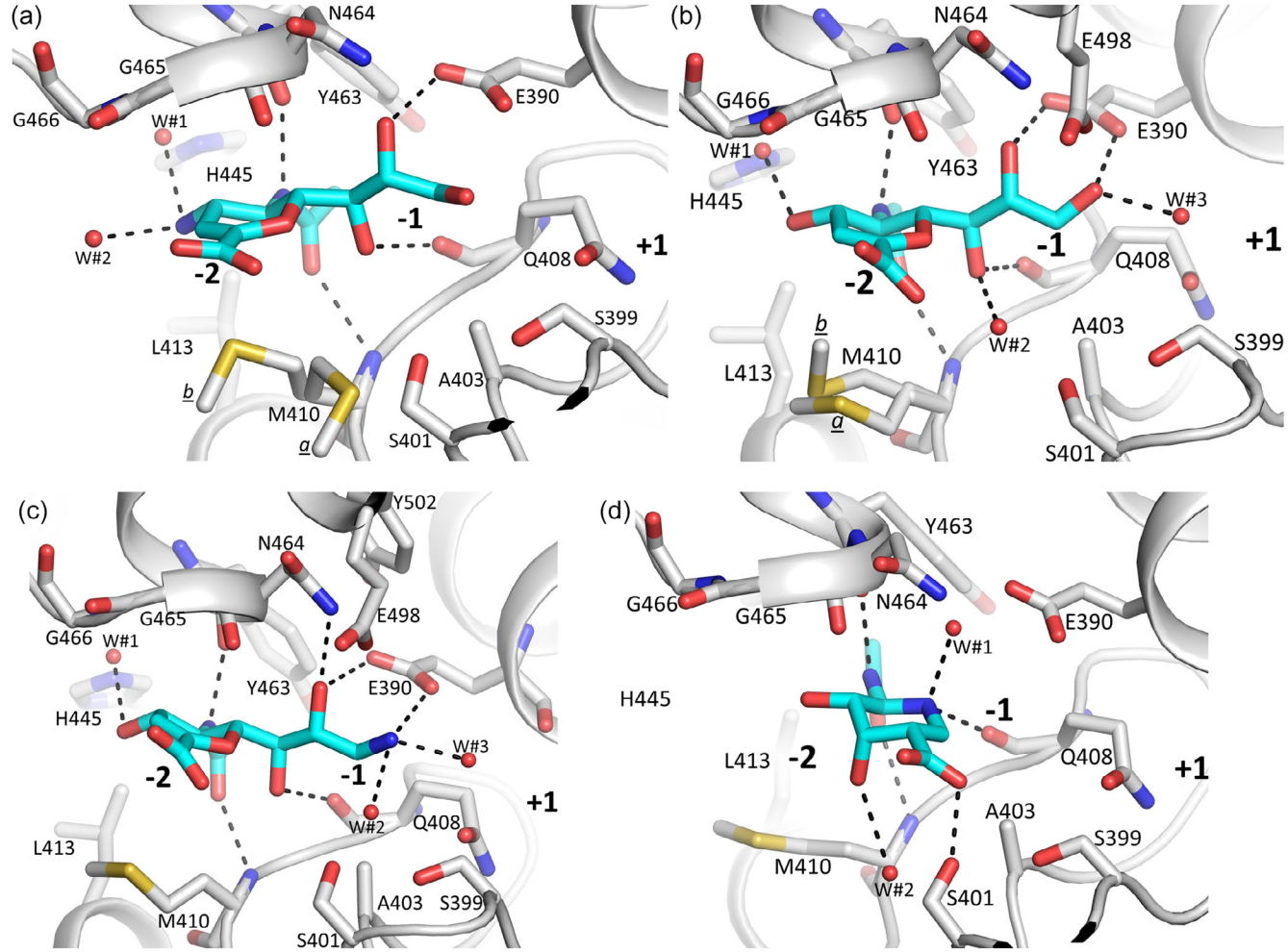

FIGURE 7 Interactions of siastatin B and deoxy-neuraminic acid analogs bound in the Cj0843c active site. Protein and inhibitor representations are as in Figure 5. Panels (a–d), same inhibitors as in Figure 4a–d.

subsite (Supporting Information: Figure S5). Third, the B-factor comparison of Z7285 indicated that GlcNAc binding to the +1 subsite is more ordered than in the −2 subsite (Supporting Information: Figure S6). In addition to these possibly mechanistically-relevant PG GlcNAc subsite binding differences, our inhibition studies also suggest that the protonation state of E390 can be modulated by different ligands. We hypothesize that E390 was protonated/neutral when bound to 10 mM Z7285 yet was deprotonated/charged when bound to Fv17b. These results complement our previous mechanistic Cj0843c studies on PG binding and varying protonation states for E390 (Kumar, Mathure, et al., 2021; Vijayaraghavan et al., 2018).

In summary, our studies have provided novel opportunities for LT inhibition. First, we have shown that relatively easy-to-synthesize O4 analogs of GlcNAc can target both the −2 −1 and the +1 +2 subsite regions of Cj0843c. Second, in addition to the −2 −1 subsite that bulgecin A binds to, the +1 +2 subsite can also be targeted for LT inhibition, with our data suggesting the latter subsite having a likely higher affinity for GlcNAc analogs. Third, modifications of GlcNAc at the 4 and 6 positions can improve inhibition of Cj0843c and could be explored for other LTs. Fourthly, the finding that known sialidase inhibitors can bind Cj0843c by positioning their N-acetyl group in the −2 subsite pocket and having additional moieties make interactions in the −1 subsite suggest they could be starting points for future LT inhibitor design. Finally, our structural comparison suggests that some of the inhibitors could also bind other LTs possibly enhancing the broader impact of these inhibitors.

4 | MATERIALS AND METHODS

4.1 | Compounds

Compounds 4-nitrophenyl N,N′-diacetyl-β-D-chitobioside, N-acetyl-2,3-dehydro-2-deoxyneuraminic acid, and

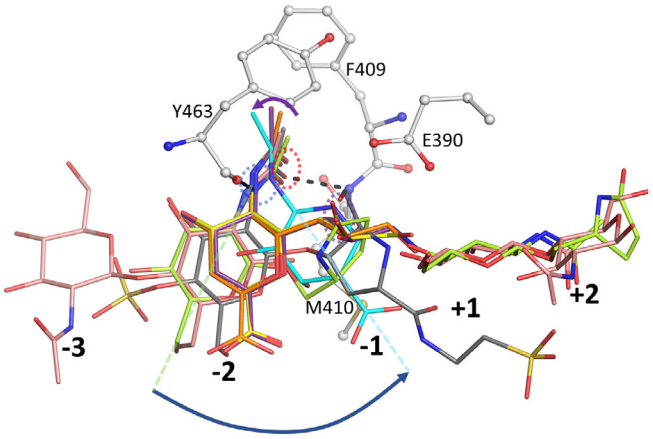

FIGURE 8 Superposition of N-acetyl-group containing compounds bound in the −2 −1 subsites of Cj0843c. The following molecules are shown with the color of their carbon atoms listed in parentheses: GlcNAc disaccharide (PDBid 7LAQ; Kumar, Mathure, et al., 2021; pink; also bound in +1 and +2 subsites), bulgecin A (PDBid 6CFC; Vijayaraghavan et al., 2018, dark gray), zanamivir amine (orange), N-acetyl-2,3-dehydro-2-deoxyneuraminic acid (yellow), Z7285 (green; also bound in +1 and + 2 subsites), Fv32r (purple), and siastatin B (cyan). Key nearby protein residues are shown in ball-and-stick representation (with gray carbon atoms). The range of different orientations of the N-acetyl-substituted ring containing compounds in the active site pivoting around the N-acetyl amide moiety is indicated by the purple arrow (for the methyl group of the N-acetyl moiety) and blue arrow (for the 6-membered ring). The approximate pivot point of the amide moiety of the compounds N-acetyl group is indicated by the blue dotted oval and red dotted oval for the amide's nitrogen and oxygen atoms, respectively, interacting with the main chain oxygen of Y463 and main chain nitrogen of M410, respectively.

siastatin B were purchased from Sigma-Aldrich. Zanamivir amine was purchased from Toronto Research Chemicals. Bulgecin A was a kind gift from Andy-Mark Thunnissen (University of Groningen).

4.2 | Design of GlcNAc derivatives

Starting with a GlcNAc moiety is hypothesized to give the inhibitors an initial affinity since both the PG substrate, model di- and trisaccharide PG mimics, and bulgecin A have a GlcNAc moiety positioned in the −2 and/or +1 subsites (Kumar, Mathure, et al., 2021; Vijayaraghavan et al., 2018). GlcNAc analogs varying at the anomeric O1 position can be synthesized using nucleophilic substitution reaction involving chloride-substituted GlcNAc and an alcohol (Guo et al., 2011). We computationally tested many GlcNAc derivatives that could be generated using alcohols with a single hydroxyl group present in commercially available alcohol compound libraries from WuXi AppTec and Enamine Ltd. Docking calculations to probe compound binding to Cj0843c were done using Schrodinger's GLIDE package (Friesner et al., 2006) as done previously (Vijayaraghavan et al., 2016). Additionally, MD simulations to probe the stability of ligand complex were carried out using Schrodinger's DESMOND package (Bowers et al., 2006) as done previously (Kumar, Mathure, et al., 2021; Kumar, Viviani, et al., 2021). Compounds were computationally tested both in the −2 −1 subsites (with the GlcNAc in the −2 subsite) and the +1 +2 subsites (with GlcNAc in the +1 subsite) as guided by our previous structural work of GlcNAc-GlcNAc disaccharide binding to Cj0843 (Kumar, Mathure, et al., 2021).

4.3 | Synthesis of GlcNAc derivatives

The following compounds were synthesized by WuXi AppTech; the final product was analyzed by liquid chromatography–mass spectrometry (LCMS) and nuclear magnetic resonance (NMR) (purity, as assessed by LC, is listed in brackets): LV8036 (100%), LV8044 (99.5%), LV8060 (100%), Fv16b (96.9%), Fv17b (100%), and Fv32r (93.7%). LCMS data and NMR spectra are in Supporting Information: Figure S2. Synthesis of the GlcNAc derivatives LV8036, LV8044, and LV8060 started from the commercially available acetyl-protected and chloro-substituted-GlcNAc compound and involved the 2-methyl-4,5-(3,4,6-tri-O-acetyl-2-deoxy-α-D-glucopyrano)-Δ2-oxazoline intermediate (Seth & Prakash, 2015; Supporting Information: Scheme 1). The more complex synthesis of Fv16b, Fv17b, and Fv32r carried out by WuXi AppTec is described in Supporting Information: Figure S3.

The following compounds were synthesized by Enamine Ltd in a similar manner and likewise characterized: Z7146 (100%), Z7912 (∼91%), Z7285 (95%), Z3252 (100%), and Z3261 (100%) (Supporting Information: Figure S2).

4.4 | Protein purification of Cj0843c

Purification of Cj0843c for crystallization and activity measurements was carried out using His-tag purification, and size-exclusion chromatography as previously described (Kumar, Mathure, et al., 2021; Vijayaraghavan et al., 2018).

4.5 | Activity assay for Cj0843c

Activity assays probing small-molecule inhibition of Cj0843c were carried out using the lysozyme EnzChek assay kit (Thermo Fisher Scientific) as done previously

(Kumar, Mathure, et al., 2021). Black 96-well plates (polystyrene half area, medium binding) were used for the assay with a reaction volume of 100 μL per well. Inhibitor stock solutions were made in DMSO or water depending on compound solubility. Each 100 μL reaction contains 50 μL of buffer (100 mM Tris pH 7.5 and 100 mM NaCl), protein (5 μM final concentration), and compound (10 μL compound was included in that initial 50 μL volume at varying concentrations). The EnzChek fluorescent PG substrate was dissolved in MilliQ water to make a 1 mg/mL stock suspension, as per kit instructions, and was vortexed to ensure the substrate had not settled to the bottom, and 50 μL was added to each well to start the reaction. The plate was sealed with clear tape and placed in a plate reader at 25°C (iD3 plate reader from Molecular Devices). The fluorescence signal was measured per assay kit instructions over the course of 3 h with moderate shaking in between reads to prevent the substrate from settling at the bottom of the plate. Experiments were done in duplicate, and results were analyzed using GraphPad software. Data were plotted as the percentage of uninhibited Cj0843c activity with the no-enzyme control set as 0%. For comparison, bulgecin A was also tested for its inhibition of Cj0843c, but due to limited quantities of this natural product, only one duplicate measurement was done at 75 μM bulgecin A concentration.

4.6 | Crystallization and inhibitor soaking of Cj0843c crystals

Cj0843c protein in 10 mM HEPES pH 8.0, 200 mM ammonium acetate buffer was concentrated to 10 mg/mL and crystallized using a hanging drop vapor diffusion method in a 24-well VDX plate (Hampton Research). The reservoir solution consisted of 0.1 M sodium citrate pH 5.9 and 26% (v/v) PEG 600. The crystallization drops are comprised of 1 μL protein and 1 μL reservoir. Crystals were observed after 3 days. Most crystals were soaked for 1 h in the mother liquor buffer containing 10 mM concentration of the inhibitor and were subsequently mounted in cryo loops and flash-frozen in liquid nitrogen for x-ray diffraction analysis. The exceptions to these soaking concentrations or times are Z7912 which was soaked for 30 min at 10 mM, and Z7285, which was soaked at three different concentrations (10, 3, and 1 mM) for 1 h for crystallographic dose–response analysis.

4.7 | Synchrotron data collection and refinement of Cj0843c inhibitor complexes

Data were collected at the NSLS-II and SSRL synchrotron facilities and processed using XDS (Kabsch, 2010), except for Fv32r, which was processed using HKL-3000 (Minor et al., 2006; see Supporting Information: Table S1 for data collection statistics). The structures were solved via molecular replacement with Phaser (McCoy et al., 2007) using the apo Cj0843c coordinates as the search model (PDB ID 6CF9; Vijayaraghavan et al., 2018). Crystals of the inhibitor Cj0843c complexes diffracted to a resolution ranging from 1.83 to 2.48 Å. The structures were refined using Refmac (Murshudov et al., 2011) and PHENIX (Adams et al., 2010), and manual model building was done using COOT (Emsley & Cowtan, 2004). After initial refinement, the active site contained electron density for the inhibitors. Refinement parameters for the inhibitors were generated using AceDRG (Long et al., 2017), and the inhibitors were included in subsequent refinement steps. Additional buffer components were located in electron density maps and included in the refinement (see Supporting Information: Table S1 for refinement details). Molecular figures were generated using Pymol (www.pymol.org). Coordinates and structure factors for the inhibitor Cj0843c complexes LV8036, LV8044, LV8060, Fv16b, Fv17b, Z3252, Z3261, Z7146, Z7912, 10 mM Z7285, 3 mM Z7285, 1 mM Z7285, 4-nitrophenyl N,N′ diacetyl-β-D-chitobioside, zanamivir amine, N-acetyl-2,-3-dehydro-2-deoxyneuraminic acid, Fv32r, and siastatin B have been deposited with the Protein Data Bank with PDB ID codes 8GEZ, 8GF0, 8GF1, 8GFB, 8GFC, 8GFD, 8GFE, 8GFF, 8GFG, 8GFH, 8GFI, 8GFJ, 8GFL, 8GFM, 8GFP, 8GFQ, and 8GFS, respectively.

ACKNOWLEDGMENTS

The authors thank beamline support at NSLS and SSRL for help with data collection. The authors thank NIH Grant 1R21AI148875 (to FVDA) for funding this study. The authors thank the CWRU HPC for computational resources.

REFERENCES

Adams PD, Afonine PV, Bunkoczi G, Chen VB, Davis IW, Echols N, et al. PHENIX: a comprehensive python-based system for macromolecular structure solution. Acta Crystallogr D Biol Crystallogr. 2010;66(Pt 2):213–21. https://doi.org/10.1107/S0907444909052925

Bonis M, Williams A, Guadagnini S, Werts C, Boneca IG. The effect of bulgecin a on peptidoglycan metabolism and physiology of *Helicobacter pylori*. Microb Drug Resist. 2012;18(3):230–9. https://doi.org/10.1089/mdr.2011.0231

Bowers KJ, Chow E, Xu H, Dror RO, Eastwood MP, Gregersen BA, et al. Scalable algorithms for molecular dynamics simulations on commodity clusters. Proceedings of the ACM/IEEE conference on supercomputing (SC06); 2006 November 11–17; Tampa, FL. 2006.

Burkinshaw BJ, Deng W, Lameignere E, Wasney GA, Zhu H, Worrall LJ, et al. Structural analysis of a specialized type III

secretion system peptidoglycan-cleaving enzyme. J Biol Chem. 2015;290(16):10406–17. https://doi.org/10.1074/jbc.M115.639013

Byun B, Mahasenan KV, Dik DA, Marous DR, Speri E, Kumarasiri M, et al. Mechanism of the *Escherichia coli* MltE lytic transglycosylase, the cell-wall-penetrating enzyme for type VI secretion system assembly. Sci Rep. 2018;8(1):4110. https://doi.org/10.1038/s41598-018-22527-y

Caceres CJ, Seibert B, Cargnin Faccin F, Cardenas-Garcia S, Rajao DS, Perez DR. Influenza antivirals and animal models. FEBS Open Bio. 2022;12(6):1142–65. https://doi.org/10.1002/2211-5463.13416

Chang M, Mahasenan KV, Hermoso JA, Mobashery S. Unconventional antibacterials and adjuvants. Acc Chem Res. 2021;54(4):917–29. https://doi.org/10.1021/acs.accounts.0c00776

Cho H, Uehara T, Bernhardt TG. β-lactam antibiotics induce a lethal malfunctioning of the bacterial cell wall synthesis machinery. Cell. 2014;159(6):1300–11. https://doi.org/10.1016/j.cell.2014.11.017

Crepin S, Ottosen EN, Peters K, Smith SN, Himpsl SD, Vollmer W, et al. The lytic transglycosylase MltB connects membrane homeostasis and in vivo fitness of *Acinetobacter baumannii*. Mol Microbiol. 2018;109(6):745–62. https://doi.org/10.1111/mmi.14000

Dik DA, Fisher JF, Mobashery S. Cell-wall recycling of the Gram-negative bacteria and the nexus to antibiotic resistance. Chem Rev. 2018;118(12):5952–84. https://doi.org/10.1021/acs.chemrev.8b00277

Dik DA, Madukoma CS, Tomoshige S, Kim C, Lastochkin E, Boggess WC, et al. Slt, MltD and MltG of *Pseudomonas aeruginosa* as targets of Bulgecin a in potentiation of β-lactam antibiotics. ACS Chem Biol. 2019;14:296–303. https://doi.org/10.1021/acschembio.8b01025

Dik DA, Marous DR, Fisher JF, Mobashery S. Lytic transglycosylases: concinnity in concision of the bacterial cell wall. Crit Rev Biochem Mol Biol. 2017;52(5):503–42. https://doi.org/10.1080/10409238.2017.1337705

Dominguez-Gil T, Molina R, Alcorlo M, Hermoso JA. Renew or die: the molecular mechanisms of peptidoglycan recycling and antibiotic resistance in Gram-negative pathogens. Drug Resist Updat. 2016;28:91–104. https://doi.org/10.1016/j.drup.2016.07.002

El Meouche I, Peltier J. Toxin release mediated by the novel autolysin Cwp19 in *Clostridium difficile*. Microb Cell. 2018;5(9):421–3. https://doi.org/10.15698/mic2018.09.648

Emsley P, Cowtan K. Coot: model-building tools for molecular graphics. Acta Crystallogr D Biol Crystallogr. 2004;60(Pt 12 Pt 1):2126–32.

Fibriansah G, Gliubich FI, Thunnissen AM. On the mechanism of peptidoglycan binding and cleavage by the endo-specific lytic transglycosylase MltE from *Escherichia coli*. Biochemistry. 2012;51(45):9164–77. https://doi.org/10.1021/bi300900t

Friesner RA, Murphy RB, Repasky MP, Frye LL, Greenwood JR, Halgren TA, et al. Extra precision glide: docking and scoring incorporating a model of hydrophobic enclosure for protein-ligand complexes. J Med Chem. 2006;49(21):6177–96.

Guo Y, Li X, Zhao Y, Si Y, Zhu H, Yang Y. Synthesis and biological evaluation of two salidroside analogues in the PC12 cell model exposed to hypoglycemia and serum limitation. Chem Pharm Bull. 2011;59(8):1045–7. https://doi.org/10.1248/cpb.59.1045

Hol WG. The role of the alpha-helix dipole in protein function and structure. Prog Biophys Mol Biol. 1985;45(3):149–95. https://doi.org/10.1016/0079-6107(85)90001-x

Horsman ME, Marous DR, Li R, Oliver RA, Byun B, Emrich SJ, et al. Whole-genome shotgun sequencing of two β-proteobacterial species in search of the bulgecin biosynthetic cluster. ACS Chem Biol. 2017;12(10):2552–7. https://doi.org/10.1021/acschembio.7b00687

Imada A, Kintaka K, Nakao M, Shinagawa S. Bulgecin, a bacterial metabolite which in concert with β-lactam antibiotics causes bulge formation. J Antibiot. 1982;35(10):1400–3.

Kabsch W. Xds. Acta Crystallogr D Biol Crystallogr. 2010;66(Pt 2):125–32. https://doi.org/10.1107/S0907444909047337

Keil JM, Rafn GR, Turan IM, Aljohani MA, Sahebjam-Atabaki R, Sun XL. Sialidase inhibitors with different mechanisms. J Med Chem. 2022;65(20):13574–93. https://doi.org/10.1021/acs.jmedchem.2c01258

Kim C, Tomoshige S, Lee M, Zgurskaya HI, Mobashery S. Penetration through outer membrane and efflux potential in *Pseudomonas aeruginosa* of bulgecin A as an adjuvant to beta-lactam antibiotics. Antibiotics. 2023;12(2):358. https://doi.org/10.3390/antibiotics12020358

Knilans KJ, Hackett KT, Anderson JE, Weng C, Dillard JP, Duncan JA. *Neisseria gonorrhoeae* lytic transglycosylases LtgA and LtgD reduce host innate immune signaling through TLR2 and NOD2. ACS Infect Dis. 2017;3(9):624–33. https://doi.org/10.1021/acsinfecdis.6b00088

Kraft AR, Prabhu J, Ursinus A, Holtje JV. Interference with murein turnover has no effect on growth but reduces β-lactamase induction in *Escherichia coli*. J Bacteriol. 1999;181(23):7192–8.

Kudo T, Nishimura Y, Kondo S, Takeuchi T. Syntheses of the potent inhibitors of neuraminidase, N-(1,2-dihydroxypropyl) derivatives of siastatin B and its 4-deoxy analogs. J Antibiot. 1993;46(2):300–9. https://doi.org/10.7164/antibiotics.46.300

Kumar V, Mathure SA, Lee M, Boorman J, Zeng X, Lin J, et al. Turnover chemistry and structural characterization of the Cj0843c lytic transglycosylase of *Campylobacter jejuni*. Biochemistry. 2021;60(14):1133–44. https://doi.org/10.1021/acs.biochem.1c00027

Kumar V, Viviani SL, Ismail J, Agarwal S, Bonomo RA, van den Akker F. Structural analysis of the boronic acid β-lactamase inhibitor vaborbactam binding to *Pseudomonas aeruginosa* penicillin-binding protein 3. PLoS One. 2021;16(10):e0258359. https://doi.org/10.1371/journal.pone.0258359

Laborda P, Wang SY, Voglmeir J. Influenza neuraminidase inhibitors: synthetic approaches, derivatives and biological activity. Molecules. 2016;21(11):E1513. https://doi.org/10.3390/molecules21111513

Lee M, Batuecas MT, Tomoshige S, Dominguez-Gil T, Mahasenan KV, Dik DA, et al. Exolytic and endolytic turnover of peptidoglycan by lytic transglycosylase Slt of *Pseudomonas aeruginosa*. Proc Natl Acad Sci U S A. 2018;115(17):4393–8. https://doi.org/10.1073/pnas.1801298115

Lee M, Hesek D, Llarrull LI, Lastochkin E, Pi H, Boggess B, et al. Reactions of all *Escherichia coli* lytic transglycosylases with bacterial cell wall. J Am Chem Soc. 2013;135(9):3311–4. https://doi.org/10.1021/ja309036q

Long F, Nicholls RA, Emsley P, Graaeulis S, Merkys A, Vaitkus A, et al. AceDRG: a stereochemical description generator for ligands. Acta Crystallogr D Struct Biol. 2017;73(Pt 2):112–22. https://doi.org/10.1107/S2059798317000067

Lorenz U, Lorenz B, Schmitter T, Streker K, Erck C, Wehland J, et al. Functional antibodies targeting IsaA of *Staphylococcus aureus* augment host immune response and open new perspectives for antibacterial therapy. Antimicrob Agents Chemother. 2011;55(1):165–73. https://doi.org/10.1128/AAC.01144-10

Magesh S, Moriya S, Suzuki T, Miyagi T, Ishida H, Kiso M. Design, synthesis, and biological evaluation of human sialidase inhibitors. Part 1: selective inhibitors of lysosomal sialidase (NEU1). Bioorg Med Chem Lett. 2008;18(2):532–7. https://doi.org/10.1016/j.bmcl.2007.11.084

Martinez-Bond EA, Soriano BM, Williams AH. The mechanistic landscape of lytic transglycosylase as targets for antibacterial therapy. Curr Opin Struct Biol. 2022;77:102480. https://doi.org/10.1016/j.sbi.2022.102480

McCoy AJ, Grosse-Kunstleve RW, Adams PD, Winn MD, Storoni LC, Read RJ. Phaser crystallographic software. J Appl Crystallogr. 2007;40(Pt 4):658–74.

Mezoughi AB, Costanzo CM, Parker GM, Behiry EM, Scott A, Wood AC, et al. The lysozyme inhibitor thionine acetate is also an inhibitor of the soluble lytic transglycosylase Slt35 from *Escherichia coli*. Molecules. 2021;26(14):4189. https://doi.org/10.3390/molecules26144189

Minor W, Cymborowski M, Otwinowski Z, Chruszcz M. HKL-3000: the integration of data reduction and structure solution—from diffraction images to an initial model in minutes. Acta Crystallogr D Biol Crystallogr. 2006;62(Pt 8):859–66. https://doi.org/10.1107/S0907444906019949

Murshudov GN, Skubak P, Lebedev AA, Pannu NS, Steiner RA, Nicholls RA, et al. REFMAC5 for the refinement of macromolecular crystal structures. Acta Crystallogr D Biol Crystallogr. 2011;67(Pt 4):355–67. https://doi.org/10.1107/S0907444911001314

Nakao M, Yukishige K, Kondo M, Imada A. Novel morphological changes in gram-negative bacteria caused by combination of bulgecin and cefmenoxime. Antimicrob Agents Chemother. 1986;30(3):414–7.

Nocadello S, Minasov G, Shuvalova LS, Dubrovska I, Sabini E, Anderson WF. Crystal structures of the SpoIID lytic transglycosylases essential for bacterial sporulation. J Biol Chem. 2016;291(29):14915–26. https://doi.org/10.1074/jbc.M116.729749

Perez Medina KM, Dillard JP. Antibiotic targets in gonococcal cell wall metabolism. Antibiotics. 2018;7(3):E64. https://doi.org/10.3390/antibiotics7030064

Ragland SA, Schaub RE, Hackett KT, Dillard JP, Criss AK. Two lytic transglycosylases in *Neisseria gonorrhoeae* impart resistance to killing by lysozyme and human neutrophils. Cell Microbiol. 2017;19(3):e12662. https://doi.org/10.1111/cmi.12662

Reid CW, Blackburn NT, Clarke AJ. The effect of NAG-thiazoline on morphology and surface hydrophobicity of *Escherichia coli*. FEMS Microbiol Lett. 2004;234(2):343–8. https://doi.org/10.1016/j.femsle.2004.03.047

Reid CW, Blackburn NT, Legaree BA, Auzanneau FI, Clarke AJ. Inhibition of membrane-bound lytic transglycosylase B by NAG-thiazoline. FEBS Lett. 2004;574(1–3):73–9. https://doi.org/10.1016/j.febslet.2004.08.006

Romeis T, Vollmer W, Holtje JV. Characterization of three different lytic transglycosylases in *Escherichia coli*. FEMS Microbiol Lett. 1993;111(2–3):141–6.

Roure S, Bonis M, Chaput C, Ecobichon C, Mattox A, Barriere C, et al. Peptidoglycan maturation enzymes affect flagellar functionality in bacteria. Mol Microbiol. 2012;86(4):845–56. https://doi.org/10.1111/mmi.12019

Scheurwater E, Reid CW, Clarke AJ. Lytic transglycosylases: bacterial space-making autolysins. Int J Biochem Cell Biol. 2008;40(4):586–91. https://doi.org/10.1016/j.biocel.2007.03.018

Seth PO, Prakash TP. Patent (WO 2015/042447 A1). 2015.

Skalweit MJ, Li M. Bulgecin A as a β-lactam enhancer for carbapenem-resistant *Pseudomonas aeruginosa* and carbapenem-resistant *Acinetobacter baumannii* clinical isolates containing various resistance mechanisms. Drug des Devel Ther. 2016;10:3013–20. https://doi.org/10.2147/DDDT.S110193

Smith BJ, Colman PM, Von Itzstein M, Danylec B, Varghese JN. Analysis of inhibitor binding in influenza virus neuraminidase. Protein Sci. 2001;10(4):689–96. https://doi.org/10.1110/ps.41801

Tailford LE, Owen CD, Walshaw J, Crost EH, Hardy-Goddard J, Le Gall G, et al. Discovery of intramolecular trans-sialidases in human gut microbiota suggests novel mechanisms of mucosal adaptation. Nat Commun. 2015;6:7624. https://doi.org/10.1038/ncomms8624

Templin MF, Edwards DH, Holtje JV. A murein hydrolase is the specific target of bulgecin in *Escherichia coli*. J Biol Chem. 1992;267(28):20039–43.

Thunnissen AM, Rozeboom HJ, Kalk KH, Dijkstra BW. Structure of the 70-kDa soluble lytic transglycosylase complexed with bulgecin A. Implications for the enzymatic mechanism. Biochemistry. 1995;34(39):12729–37.

Tomoshige S, Dik DA, Akabane-Nakata M, Madukoma CS, Fisher JF, Shrout JD, et al. Total syntheses of bulgecins A, B, and C and their bactericidal potentiation of the β-lactam antibiotics. ACS Infect Dis. 2018;4(6):860–7. https://doi.org/10.1021/acsinfecdis.8b00105

van Asselt EJ, Kalk KH, Dijkstra BW. Crystallographic studies of the interactions of *Escherichia coli* lytic transglycosylase Slt35 with peptidoglycan. Biochemistry. 2000;39(8):1924–34.

van Asselt EJ, Thunnissen AM, Dijkstra BW. High resolution crystal structures of the *Escherichia coli* lytic transglycosylase Slt70 and its complex with a peptidoglycan fragment. J Mol Biol. 1999;291(4):877–98. https://doi.org/10.1006/jmbi.1999.3013

Vijayaraghavan J, Kramp K, Harris ME, van den Akker F. Inhibition of soluble guanylyl cyclase by small molecules targeting the catalytic domain. FEBS Lett. 2016;590(20):3669–80. https://doi.org/10.1002/1873-3468.12427

Vijayaraghavan J, Kumar V, Krishnan NP, Kaufhold RT, Zeng X, Lin J, et al. Structural studies and molecular dynamics simulations suggest a processive mechanism of exolytic lytic transglycosylase from *Campylobacter jejuni*. PLoS One. 2018;13(5):e0197136. https://doi.org/10.1371/journal.pone.0197136

Weaver AI, Alvarez L, Rosch KM, Ahmed A, Wang GS, van Nieuwenhze MS, et al. Lytic transglycosylases mitigate periplasmic crowding by degrading soluble cell wall turnover products. Elife. 2022;11:e73178. https://doi.org/10.7554/eLife.73178

Williams AH, Wheeler R, Thiriau C, Haouz A, Taha MK, Boneca IG. Bulgecin A: the key to a broad-spectrum inhibitor that targets lytic transglycosylases. Antibiotics. 2017;6(1):E8. https://doi.org/10.3390/antibiotics6010008

Wu CJ, Huang YW, Lin YT, Yang TC. Inactivation of lytic transglycosylases increases susceptibility to aminoglycosides and macrolides by altering the outer membrane permeability of *Stenotrophomonas maltophilia*. Antimicrob Agents Chemother. 2016;60(5):3236–9. https://doi.org/10.1128/AAC.03026-15

Wydau-Dematteis S, El Meouche I, Courtin P, Hamiot A, Lai-Kuen R, Saubamea B, et al. Cwp19 is a novel lytic transglycosylase involved in stationary-phase autolysis resulting in toxin release in *Clostridium difficile*. mBio. 2018;9(3):e00648-18. https://doi.org/10.1128/mBio.00648-18

Zahrl D, Wagner M, Bischof K, Bayer M, Zavecz B, Beranek A, et al. Peptidoglycan degradation by specialized lytic transglycosylases associated with type III and type IV secretion systems. Microbiology. 2005;151(Pt 11):3455–67. https://doi.org/10.1099/mic.0.28141-0

Zeng X, Gillespie B, Lin J. Important role of a putative lytic transglycosylase Cj0843c in β-lactam resistance in *Campylobacter jejuni*. Front Microbiol. 2015;6:1292. https://doi.org/10.3389/fmicb.2015.01292

Zeng X, Lin J. β-lactamase induction and cell wall metabolism in Gram-negative bacteria. Front Microbiol. 2013;4:128. https://doi.org/10.3389/fmicb.2013.00128

SUPPORTING INFORMATION

Additional supporting information can be found online in the Supporting Information section at the end of this article.

How to cite this article: Kumar V, Boorman J, Greenlee WJ, Zeng X, Lin J, van den Akker F. Exploring the inhibition of the soluble lytic transglycosylase Cj0843c of *Campylobacter jejuni* via targeting different sites with different scaffolds. Protein Science. 2023;32(7):e4683. https://doi.org/10.1002/pro.4683